Annals of Pharmacy Practice and Pharmacotherapy
ISSN: 3062-4436
2025, Volume 5, Page No: 53-66

Available online at: www.galaxypub.co/page/journals

Galaxy Publication

Galaxy Publication

Design, Characterization, Initial Molecular Docking, Pharmacological Evaluation, and ADME Profiling of Novel Pyrazoline Derivatives as Potential Anti-Breast Cancer Agents

Eva Schmidt[1], Max Bauer[1]*, Lena Richter[1]

[1]Institute of Pharmaceutical Sciences, Humboldt University of Berlin, Berlin, Germany.

***E-mail** ✉ max.bauer@yahoo.com

Received: 09 January 2025; **Revised:** 29 March 2025; **Accepted:** 11 April 2025

ABSTRACT

The present study explored the anti-breast cancer properties of novel pyrazoline-substituted benzenesulfonamides (6–10) through computational and laboratory approaches. Molecular docking analyses using the GOLD suite were performed on the human estrogen receptor and the PARP1 antagonist crystal structure, with tamoxifen serving as the reference compound, yielding comparable binding results. In vitro evaluation on MCF-7 and MDA-MB-468 breast cancer cell lines revealed that these compounds exerted dose-dependent antiproliferative effects. Among them, compound 9 showed the highest docking affinity against the PARP1 antagonist in triple-negative breast cancer, with a PLP fitness score of 93.24, and inhibited MDA-MB-468 cell proliferation with an IC50 of 2.79 µM. Compounds 8 and 10 were particularly effective against MCF-7 cells, exhibiting IC50 values of 7.4 µM and 17.96 µM, respectively, highlighting their potential as targeted anti-breast cancer agents.

Keywords: ADME evaluation, Triple-negative breast cancer, Pyrazole, Antiproliferative, Molecular docking

How to Cite This Article: Schmidt E, Bauer M, Richter L. Design, Characterization, Initial Molecular Docking, Pharmacological Evaluation, and ADME Profiling of Novel Pyrazoline Derivatives as Potential Anti-Breast Cancer Agents. Ann Pharm Pract Pharmacother. 2025;5:53-66. https://doi.org/10.51847/GKdnvc0hG5

Introduction

Cancer continues to pose one of the most critical health threats worldwide and remains a leading cause of death [1]. Despite advances in modern medicine, effective treatment strategies for cancer are still limited, emphasizing the need for novel and safer anticancer agents with potent activity against tumor cells [2]. Among cancers, breast cancer (BC) is particularly deadly and represents a major global health burden [3]. A majority of BC cases—approximately 80%—are classified as estrogen receptor-positive (ER+) due to the overexpression of the estrogen receptor [4–6]. The human estrogen receptor alpha (hER) plays an essential role in regulating key physiological processes, including cell proliferation, survival, and metastatic progression in cancer [7–9].

In contrast, triple-negative breast cancer (TNBC), accounting for roughly 10%–15% of BC cases, lacks expression of ER, progesterone receptor (PR), and human epidermal growth factor receptor 2 (HER2), but shows elevated levels of poly ADP ribose polymerase 1 (PARP1) [10]. One of the main obstacles in treating BC is the emergence of multi-drug resistance and insufficient selectivity of conventional therapies, prompting extensive research into the development of highly selective molecules capable of effectively suppressing tumor growth.

Heterocyclic compounds, both naturally occurring and synthetic, constitute a cornerstone of medicinal chemistry due to their involvement in numerous vital biological processes [11]. Aromatic heterocycles, in particular, are frequently incorporated into bioactive molecules for their pharmacological potential. Pyrazoline, a five-membered heterocycle containing two nitrogen atoms, stands out for its wide-ranging chemical and biological properties, as well as its relevance in drug design [12, 13]. Previous research has highlighted the pyrazoline scaffold as a versatile platform for the synthesis of new compounds with promising anticancer activities [14]. **Figure 1**

illustrates several examples of drugs containing pyrazoline motifs that exhibit notable anticancer effects [9, 15–18].

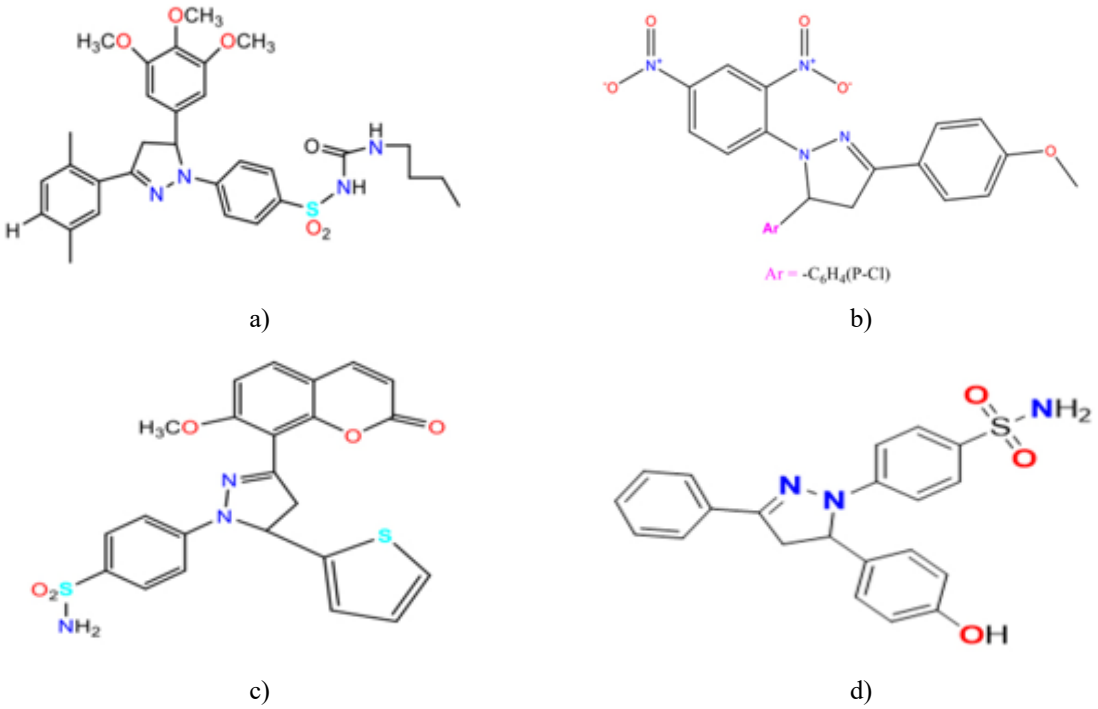

Figure 1. Several synthetic compounds incorporating pyrazoline scaffolds have demonstrated notable anticancer potential. Due to their cytotoxic properties, sulfonamide-derived compounds, including pyrazoles and pyrazolines, have garnered significant interest in medicinal research [19]. Researchers are actively engaged in the design, molecular docking, synthesis, characterization, and in vitro evaluation of new pyrazoline derivatives containing a sulfonamide moiety for anticancer activity.

Materials and Methods

Chemicals and reagents

All chemicals and commonly used intermediates were procured from commercial suppliers, including BDH (UK) and Sigma-Aldrich (Germany), as well as Hyper-Chem and Hangxing RD (Hangzhou, China).

Characterization techniques

Melting points were determined using the capillary method on a Bamstead/Electrothermal 9100 apparatus (UK). Infrared spectra were recorded as KBr disks using a Fourier Transform Infrared Spectrophotometer (FTIR-6100 Type A). Proton NMR (^{1}H-NMR) spectra were acquired at 500 MHz using a Varian Agilent instrument, while carbon NMR (^{13}C-NMR) spectra were obtained at 125 MHz on an Agilent system.

Synthesis of molecular structures

Various novel pyrazoline derivatives were synthesized following the methods illustrated in Scheme 1.

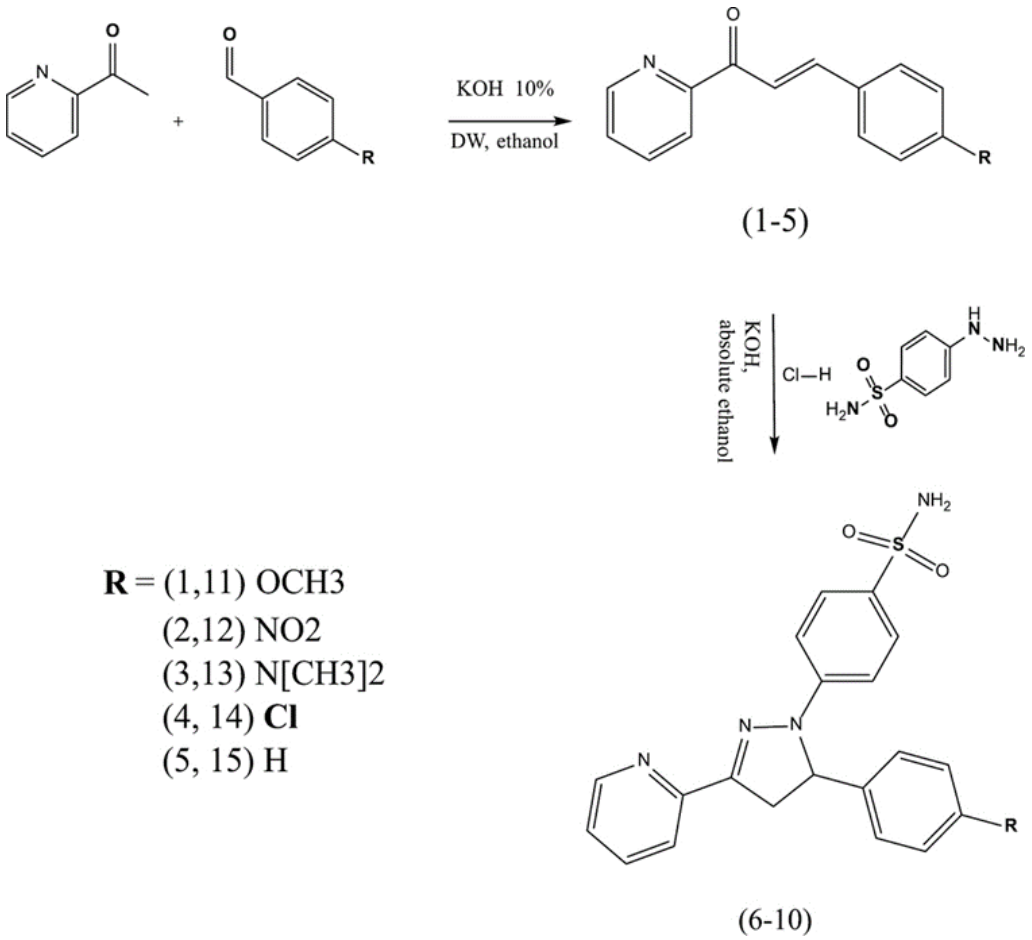

Scheme 1. Representation of the synthesis pathway for final compounds (6–10).

Synthesis of chalcone derivatives (1–5)

Intermediate chalcone derivatives were prepared through Claisen–Schmidt condensation of the corresponding 4-substituted benzaldehydes with 2-acetylpyridine, following the procedure reported by Eid and George (2018) [20]. Method A was employed to produce compounds 2 and 4, which are chalcones bearing nitro and chloro substituents. 2-Acetylpyridine was added gradually over 2–3 hours to a mixture containing 10 mL of 10% aqueous sodium hydroxide, 5 mL of ethanol, and the relevant aldehydes (4-nitrobenzaldehyde and 4-chlorobenzaldehyde, 17 mmol and 1.90 mL, respectively) while maintaining the temperature at 0 °C. After stirring for an additional 2 hours, the solid product was collected via filtration and washed thoroughly with distilled water.

Method B was applied to synthesize compounds 1, 3, and 5. Here, 17 mmol each of 2-acetylpyridine and the corresponding benzaldehydes (4-methoxybenzaldehyde, 4-dimethylaminobenzaldehyde, and benzaldehyde) were added to 100 mL of water at temperatures below 5 °C. The mixture was vigorously stirred to form a fine emulsion, followed by the slow addition of 10 mL of 10% sodium hydroxide solution. After two rounds of thorough mixing, the reaction mixture was left undisturbed overnight at 4 °C. Agitation was avoided to prevent phase separation, which reduces yield. The product was separated into an oily phase that eventually solidified, after which it was filtered and washed with ample distilled water.

General procedure for pyrazoline derivatives (6–10)

Equimolar amounts of the chalcone derivatives (1–5) (2 mmol) and 4-hydrazine benzenesulfonamide hydrochloride (2 mmol, 0.8947 g) were dissolved in 5 mL of absolute ethanol, followed by the addition of potassium hydroxide (5 mmol, 0.28 g). The reaction mixture was refluxed for 8 hours, then cooled, and the resulting precipitate was isolated by filtration and washed extensively with distilled water [21].

Compound 1: (E)-3-(4-Methoxyphenyl)-1-(pyridin-2-yl)prop-2-en-1-one

This compound appears as a green powder with a melting point of 79–80 °C and a yield of 87%. IR spectroscopy showed characteristic absorptions at 3057.27 cm^{-1} (aromatic C–H), 2974.33 and 2841.24 cm^{-1} (O–CH_3), 1666.55

cm^{-1} (C=O), 1599.04 cm^{-1} (C=C of alkene), 1570.1 and 1520.3 cm^{-1} (aromatic C=C and C=N), and 1259.56 cm^{-1} (C–O–CH_3). The ^1H NMR spectrum (500 MHz, DMSO, δ) displayed signals at 3.80 (3H, s, OCH_3), 7.00–7.02 (1H, d, α-vinyl proton), 7.14–7.65 (5H, m, aromatic H), 8.00–8.03 (1H, d, β-vinyl proton), and 8.07–8.78 (3H, m, aromatic H). The ^{13}C NMR spectrum (125 MHz, DMSO-d_6) showed peaks at 55.83 (O–CH_3), 115.30–162.00 (11 aromatic C), 122.83 (C=C adjacent to C=O), 144.5 (C=C adjacent to aromatic ring), and 188.95 (C=O).

Compound 2: (E)-3-(4-Nitrophenyl)-1-(pyridin-2-yl)prop-2-en-1-one

This derivative is obtained as a light brown powder with a melting point of 153–154 °C and a yield of 77%. IR absorptions include 3057.27 cm^{-1} (aromatic C–H), 1666.55 cm^{-1} (C=O), 1604.83 cm^{-1} (C=C of alkene), 1589.40 and 1514.17 cm^{-1} (aromatic C=C and C=N), and 1344.43 cm^{-1} (NO_2 group). The ^1H NMR spectrum (500 MHz, DMSO, δ) showed signals at 7.72 (1H, d, α-vinyl proton), 7.88–8.04 (3H, m, aromatic H), 8.05–8.06 (1H, d, β-vinyl proton), and 8.07–8.80 (5H, m, aromatic H). The ^{13}C NMR spectrum (125 MHz, DMSO-d_6) exhibited peaks at 123.09–153.46 (11 aromatic C), 130.19 (C=C adjacent to C=O), 141.39 (C=C adjacent to aromatic ring), and 189.01 (C=O).

Compound 3: (E)-3-(4-(Dimethylamino)phenyl)-1-(pyridin-2-yl)prop-2-en-1-one

This compound is obtained as a light orange powder with a melting point of 82–83 °C and a yield of 85%. Its IR spectrum displays absorptions at 3041.84 cm^{-1} (aromatic C–H), 2910.68 and 2804.59 cm^{-1} (CH_3), 1668.48 cm^{-1} (C=O), 1599.04 cm^{-1} (C=C of alkene), 1539.25 and 1437.02 cm^{-1} (aromatic C=C and C=N), and 1165.04 cm^{-1} (N–CH_3). The ^1H NMR spectrum (500 MHz, DMSO, δ) exhibits signals at 3.00 (6H, s, $N(CH_3)_2$), 6.66–6.73 (1H, d, α-vinyl proton), 7.62–7.64 (4H, m, aromatic H), 7.66–7.68 (1H, d, β-vinyl proton), and 7.77–8.76 (4H, m, aromatic H). The ^{13}C NMR spectrum (125 MHz, DMSO-d_6) shows peaks at 40.12 (N–CH_3), 111.51–154.65 (11 aromatic C), 122.64 (C=C adjacent to C=O), 149.46 (C=C adjacent to aromatic ring), and 190.29 (C=O).

Compound 4: (E)-3-(4-Chlorophenyl)-1-(pyridin-2-yl)prop-2-en-1-one

This substance appears as a light green powder with a melting point of 94–96 °C and a yield of 79%. The IR spectrum shows characteristic peaks at 3057.27 cm^{-1} (aromatic C–H), 1674.27 cm^{-1} (C=O), 1606.76 cm^{-1} (C=C of alkene), 1585.54 and 1492.95 cm^{-1} (aromatic C=C and C=N), and 1089.92 cm^{-1} (C–Cl). The ^1H NMR spectrum (500 MHz, DMSO) exhibits signals at 7.35–7.38 (2H, m, aromatic H), 7.46–7.48 (1H, d, α-vinyl proton), 7.66–8.07 (5H, m, aromatic H), 8.22–8.25 (1H, d, β-vinyl proton), and 8.77–8.78 (1H, m, aromatic H). The ^{13}C NMR spectrum (125 MHz, DMSO-d_6) shows peaks at 122.96–153.75 (11 aromatic C), 128.46 (C=C adjacent to C=O), 142.95 (C=C adjacent to aromatic ring), and 189.05 (C=O).

Compound 5: (E)-3-Phenyl-1-(pyridin-2-yl)prop-2-en-1-one

This derivative is a pale green powder with a melting point of 60–61 °C and a yield of 71%. Its IR spectrum displays absorptions at 3063.06 cm^{-1} (aromatic C–H), 1668.48 cm^{-1} (C=O), 1604.83 cm^{-1} (C=C of alkene), and 1585.54 and 1489.1 cm^{-1} (aromatic C=C and C=N). The ^1H NMR spectrum (500 MHz, DMSO, δ) shows signals at 7.22–7.86 (6H, m, aromatic H), 7.88–7.89 (1H, d, α-vinyl proton), 8.0–8.14 (2H, m, aromatic H), 8.2–8.30 (1H, d, β-vinyl proton), and 8.82–8.83 (1H, m, aromatic H). The ^{13}C NMR spectrum (125 MHz, DMSO-d_6) shows peaks at 123.47–156.06 (11 aromatic C), 130.32 (C=C adjacent to C=O), 146.71 (C=C adjacent to aromatic ring), and 191.36 (C=O).

Compound 6: 4-(5-(4-Methoxyphenyl)-3-(pyridin-2-yl)-4,5-dihydro-1H-pyrazol-1-yl)benzenesulfonamide

This compound is isolated as dark green crystals with a melting point of 139–141 °C and a yield of 87%. IR spectroscopy shows peaks at 3371.68 and 3271.38 cm^{-1} for NH_2 groups, 3057.27 cm^{-1} for aromatic C–H, 2966.63 and 2841.24 cm^{-1} for CH_3, 1597.11 cm^{-1} for the pyrazoline C=N bond, 1508.38 and 1465.95 cm^{-1} for aromatic C=C and C=N, and 1346.7 and 1153.9 cm^{-1} for the SO_2N group. The ^1H NMR spectrum (500 MHz, DMSO) shows signals at 3.17 (1H, dd, CH_2 pyrazoline), 3.79 (3H, s, O–CH_3), 3.94 (1H, dd, CH_2 pyrazoline), 5.62 (1H, dd, CH pyrazoline), 6.89 (2H, d, aromatic H ortho to OCH_3), 7.06 (2H, s, SO_2NH_2), and 7.13–8.86 (12H, m, aromatic H). The ^{13}C NMR spectrum (125 MHz, DMSO-d_6) displays peaks at 43.34 (C-5 pyrazoline), 55.50 (O–CH_3), 62.60 (C-4 pyrazoline), 112.89–151.34 (16 aromatic C), 146.03 (C=N of diazole), and 159.07 (aromatic C linked to O–CH_3).

Compound 7: 4-(5-(4-Nitrophenyl)-3-(pyridin-2-yl)-4,5-dihydro-1H-pyrazol-1-yl)benzenesulfonamide

This compound was isolated as dark brown crystals with a melting point of 192–194 °C and a yield of 72%. The IR spectrum shows NH_2 absorptions at 3362.04 and 3252.09 cm^{-1}, aromatic C–H at 3063.06 cm^{-1}, pyrazoline C=N at 1595.18 cm^{-1}, and aromatic C=C and C=N at 1518.03 and 1398.51 cm^{-1}. The SO_2N group is observed at 1344.43 and 1157.33 cm^{-1}. The ^1H NMR spectrum (500 MHz, DMSO) exhibits peaks at 3.05 and 3.98 (1H each, dd, CH_2 pyrazoline), 5.44 (1H, dd, CH pyrazoline), 6.96 (2H, s, SO_2NH_2), and 7.06–8.69 (12H, m, aromatic H). The ^{13}C NMR spectrum (125 MHz, DMSO-d_6) shows peaks at 41.43 ($N(CH_3)_2$), 46.22 (C-5 pyrazoline), 63.31 (C-4 pyrazoline), 108.21–144.11 (17 aromatic C), and 148.21 (C=N of diazole).

Compound 8: 4-(5-(4-(Dimethylamino)phenyl)-3-(pyridin-2-yl)-4,5-dihydro-1H-pyrazol-1-yl)benzenesulfonamide

This derivative also appears as dark brown crystals with a melting point of 192–194 °C and a 72% yield. IR absorptions include 3362.04 and 3252.09 cm^{-1} (NH_2), 3063.06 cm^{-1} (aromatic C–H), 1595.18 cm^{-1} (C=N), 1518.03 and 1398.51 cm^{-1} (aromatic C=C and C=N), and 1344.43 and 1157.33 cm^{-1} (SO_2N). The ^1H NMR spectrum (500 MHz, DMSO) shows 3.05 and 3.98 ppm (1H each, dd, CH_2 pyrazoline), 5.44 ppm (1H, dd, CH pyrazoline), 6.96 ppm (2H, s, SO_2NH_2), and 7.06–8.69 ppm (12H, m, aromatic H). The ^{13}C NMR spectrum (125 MHz, DMSO-d_6) exhibits 41.43 ppm ($N(CH_3)_2$), 46.22 ppm (C-5 pyrazoline), 63.31 ppm (C-4 pyrazoline), 108.21–144.11 ppm (17 aromatic C), and 148.21 ppm (C=N of diazole).

Compound 9: 4-(5-(4-Chlorophenyl)-3-(pyridin-2-yl)-4,5-dihydro-1H-pyrazol-1-yl)benzenesulfonamide

This compound was obtained as pale brown crystals with a melting point of 119–121 °C and a yield of 77%. The IR spectrum shows NH_2 absorptions at 3365.9 and 3292.60 cm^{-1}, aromatic C–H at 3092.82 cm^{-1}, pyrazoline C=N at 1595.48 cm^{-1}, aromatic C=C and C=N at 1494.88 and 1404.21 cm^{-1}, SO_2N at 1327.07 and 1149.61 cm^{-1}, and C–Cl at 1089.23 cm^{-1}. The ^1H NMR spectrum (500 MHz, DMSO) displays 3.23 and 3.98 ppm (CH_2 pyrazoline), 5.77 ppm (CH pyrazoline), 7.09 ppm (2H, s, SO_2NH_2), and 7.1–8.69 ppm (12H, m, aromatic H). The ^{13}C NMR spectrum (125 MHz, DMSO-d_6) shows 42.81 ppm (C-5 pyrazoline), 62.70 ppm (C-4 pyrazoline), 111.74–149.52 ppm (17 aromatic C), and 140.58 ppm (C=N pyrazoline).

Compound 10: 4-(5-Phenyl-3-(pyridin-2-yl)-4,5-dihydro-1H-pyrazol-1-yl)benzenesulfonamide

This compound appears as brown crystals with a melting point of 96–98 °C and a yield of 62%. IR absorptions are observed at 3340.82 and 3288.74 cm^{-1} (NH_2), 3061.13 cm^{-1} (aromatic C–H), 1591.33 cm^{-1} (C=N), 1502.60 and 1464.02 cm^{-1} (aromatic C=C and C=N), and 1332.68 and 1153.47 cm^{-1} (SO_2N). The ^1H NMR spectrum (500 MHz, DMSO) shows 3.22 and 3.99 ppm (CH_2 pyrazoline), 5.73 ppm (CH pyrazoline), 7.07 ppm (2H, s, SO_2NH_2), and 7.16–8.62 ppm (12H, m, aromatic H). The ^{13}C NMR spectrum (125 MHz, DMSO-d_6) shows 43.02 ppm (C-5 pyrazoline), 63.35 ppm (C-4 pyrazoline), 111.62–148.23 ppm (17 aromatic C), and 139.38 ppm (C=N pyrazoline).

Computational methods

Figure 2 illustrates the computational workflow of this study. Molecular docking was performed using CCDC GOLD Suite (v. 5.6.2), and ligand–receptor interactions, hydrogen bonds, short contacts, and bond lengths were analyzed using CCDC Hermes visualizer (v. 1.9.2). Ligand and reference drug structures were drawn using ChemBioOffice (v. 17.1). ADME properties of the synthesized compounds were predicted via the SwissADME server [21].

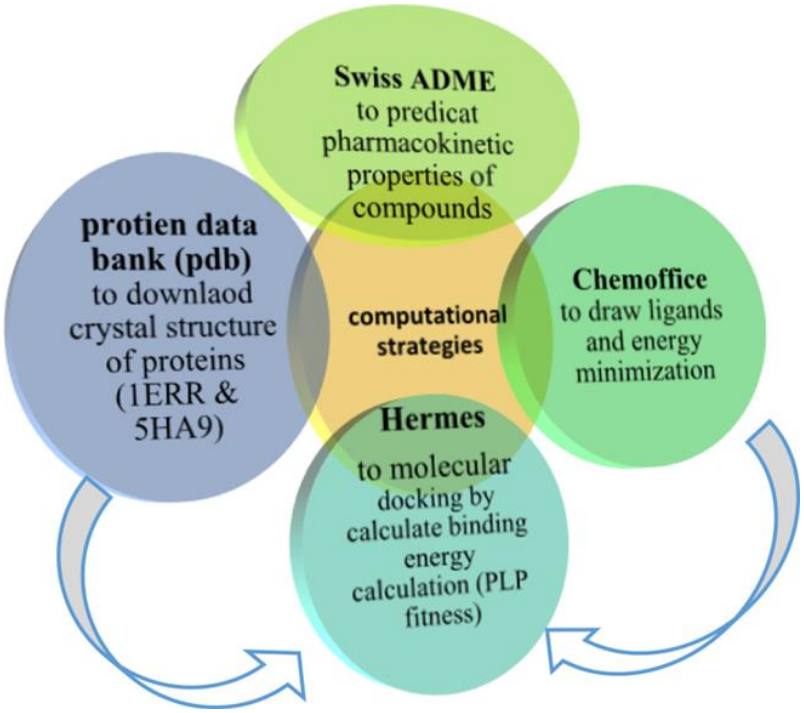

Figure 2. Computational workflow for the target compounds

ADME analysis

Compounds 6–10 were drawn using ChemBioOffice software and subsequently converted into SMILES notation via the SwissADME tool. SwissADME was also employed to predict the pharmacokinetic and physicochemical properties of the compounds. Lipophilicity and polarity of the small molecules were evaluated using the BOILED-Egg model [22].

Ligand and receptor preparation

Crystal structures of the human estrogen receptor and PARP1 antagonist were retrieved from the Protein Data Bank (PDB). Missing atoms were added using SwissPDB Viewer (SPDBV) v3.7. Water molecules not involved in ligand binding were removed, while essential ones were retained. Hydrogen atoms were incorporated to correctly ionize amino acid residues and establish tautomeric states. Energy minimization of the prepared molecules was performed using ChemBio3D v19.1 with the MM2 force field.

Molecular docking protocol

Docking studies were carried out using the licensed version of GOLD (Genetic Optimization for Ligand Docking) v2020.3.0, with the Hermes visualizer application handling the docking simulations. The docking binding site encompassed nucleotides and protein residues located within 10 Å of the reference ligands. Protein structures were obtained from PDB entries 1ERR and 5HA9. The active site radius was set at 10 Å based on the reference ligand. The ChemScore kinase configuration was used as a template, and scoring was performed using the ChemPLP function. Default parameters were applied for all GOLD settings, and docking results—including ligand poses, binding modes, and binding free energies—were analyzed to evaluate interactions with active site residues of the human estrogen receptor.

Antiproliferative assay

The cytotoxic effects of compounds 6–10 were assessed on breast cancer cell lines (MCF-7 and MDA-MB-468) using the MTT assay. This study was conducted at the College of Pharmacy, Mustansiriyah University.

Determination of half-maximal inhibitory concentration (IC_{50})

The IC_{50} values, representing the concentration required to reduce cell viability by 50%, were calculated from the MTT assay data collected 72 hours after treating the cells with compounds 6–10.

Statistical analysis

GraphPad Prism and nonlinear curve fitting software were used for statistical evaluation of the IC_{50} and MTT assay data. One-way analysis of variance (ANOVA) followed by Tukey's test was applied to compare groups on the same MTT plate. Differences were considered statistically significant at $P < 0.05$.

Results and Discussion

Analysis of ADME properties

The drug-like properties of all synthesized compounds (6–10) were evaluated using Lipinski's Rule of Five [23], a standard procedure in drug discovery for identifying promising lead molecules. According to this rule, orally active compounds should have a molecular weight ≤500, Log P ≤5, no more than 10 hydrogen bond acceptors, and no more than 5 hydrogen bond donors. Additionally, the topological polar surface area (TPSA), which influences oral bioavailability, was assessed; compounds with TPSA values above 140 Å² are predicted to have poor passive absorption. The ADME predictions indicated that all compounds except compound 7 had TPSA values below 140 Å², specifically 106.26, 142.85, 100.27, 97.03, and 97.03 Å². All compounds showed sufficient oral bioavailability with a value of 0.55, suggesting effective systemic absorption. **Table 1** summarizes Lipinski's RO5 analysis. All derivatives also satisfied key molecular descriptors related to drug-likeness, including Log P and Log S values.

Table 1. The ADME result for the final derivatives.

Comp.	H-bond acceptor	H-bond donor	MR	TPSA (A°)	GI Abs	BBB permeant	Bioavailability	Lipinski violation
6	6	1	117.54	106.26	High	NO	0.55	0 violation
7	7	1	119.87	142.85	Low	NO	0.55	0 violation
8	5	1	125.26	100.27	High	NO	0.55	0 violation
9	5	1	116.06	97.03	High	NO	0.55	0 violation
10	5	1	111.05	97.03	High	NO	0.55	0 violation

All compounds, with the exception of compound 7, exhibited high gastrointestinal (GI) absorption scores, which predict the extent of xenobiotic uptake from the gut following oral administration. These results suggest that most of the synthesized molecules are likely to be efficiently absorbed in the intestines, whereas compound 7 is expected to have limited absorption.

Analysis of docking results

Compounds 6–10 were successfully docked using the GOLD Suite software. Prior to docking, ligands were energy-minimized to correct distorted geometries by repositioning atoms and relieving internal strain, achieving a stable, low-energy conformation. The fitness of the resulting ligand–protein complexes was evaluated for all compounds. Binding affinities of compounds 6–10, as well as tamoxifen, were assessed against the human estrogen receptor (PDB: 1ERR), and compounds 6–10 were also evaluated against a PARP1 antagonist (PDB: 5HA9), using PLP fitness scores at the respective active sites. For the estrogen receptor, PLP fitness values ranged from 78.24 to 89.37, while docking with the PARP1 antagonist yielded scores between 81.62 and 93.24 **(Table 2)**. The docking analysis highlighted the formation of hydrogen bonds and other short-range interactions between the ligands and the target proteins. Distances between specific protein atoms and ligand atoms were measured, with most interactions occurring within 3 Å. These short contacts represent various non-covalent interactions, including van der Waals forces, electrostatic interactions, steric effects, π–π stacking, and dipole–dipole interactions.

Table 2. A score for docking with interactions between amino acids on both targets.

Short contact interactions	H-Bond interactions	Binding Energy (PLP Fitness)	Compounds	Protein data bank
Amino acid residues	Amino acid residues			

TRP 383, MET 343 (2), LEU 346 ARG 394 (2), GLY 521, ILE 424	HIS 524	79.37	**1**	**Human estrogen recepor PDB code: (1ERR)**
ARG 394, LEU 387, PHE 404, PHE 425 (3), ILE 424 (2), MET 421, MET 388 (3), LEU 384, LEU 525	ARG 394 (2), GLU 353, HOH Bridge with LEU 387 and GLU 353	78.24	**2**	
ILE 424 (3), HIS 524, LEU 525 (3), LEU 346 (3), LEU 391, ARG 394 , GLU 353 (2), HOH bridge with LEU 387, ARG 394 and GLU 353	GLU 353, ARG 394, HOH bridge with LEU 387 and GLU 535	89.27	**3**	
ILE 424 (2), MET 388, LEU 384 , LEU 525	THR 347	82.63	**4**	
ILE 424, LEU 349 (2), TRP 383 (2), ALA 350 (3), ASP 351	ASP 351	89. 37	**5**	
ILE 424, LEU 525 (3), LEU 391 (2), MET 388	-	94.69	**TAMOXIFEN**	
LEU 384 (4), LEU 525 (2), THR 347, MET 343, PHE 404 (3), LEU 428, LEU 387, ARG 394, GLU 353	ARG 394, GLU 353, HOH bridge with LEU 387 and GLU 353	95.36	**4-HRT**	
TYR 246, TYR 235, ASN 106 (3), ASN 207	TYR 246, ARG 204, SER 203, ASN 106 (2)	90.09	**1**	**PARP1 PDF CODE: (5HA9)**
TYR 246, ASN 106 (3), ASN 207, TYR 228	TYR 246, ASN 106 (2), SER 203, ARG 204	87.58	**2**	
TYR 228, LYS 232, ALA 219 (3), SER 243 (2), PHE 236	SER 243 (3), GLY 202, TRP 200	87.45	**3**	
TYR 246, ASN 106 (4), ASN 207, HIS 201 (4), TYR 235	TYR 246, ASN 106 (2) SER 203, ARG 204	93.24	**4**	
MET 229 (2), HIS 201 (2), ARG 204, ASN 207 (2), ASN 106 (3)	SER 203, ASN 106 (2), ARG 204	81.62	**5**	
TYR 246, HIS 201, TYR 235	-	69.80	**TP0 (reference ligand)**	

Docking studies indicated that the ligands from our final library form multiple interactions, including hydrogen bonds and short-range contacts, with key amino acids in the human estrogen alpha receptor active site, such as ALA 350, ASP 351, GLU 353, TRP 383, LEU 384, LEU 387, MET 388, LEU 391, ARG 394, PHE 404, MET 421, ILE 424, PHE 425, LEU 428, GLY 521, HIS 524, and LEU 525. These interactions highlight the potential of these compounds as anti-breast cancer agents. Among them, compounds 13 and 15 displayed the highest PLP fitness scores of 89.27 and 89.37, respectively, while reference drugs tamoxifen and 4-hydroxytamoxifen (4-HRT) scored 94.69 and 95.36. The binding mode of 4-HRT is presented in **Figure 2**, whereas **Figures 3 and 4** show the detailed interactions of high-scoring compounds 8 and 10. **Figure 5** illustrates the binding pattern of compound 9 within the PARP1 antagonist active site.

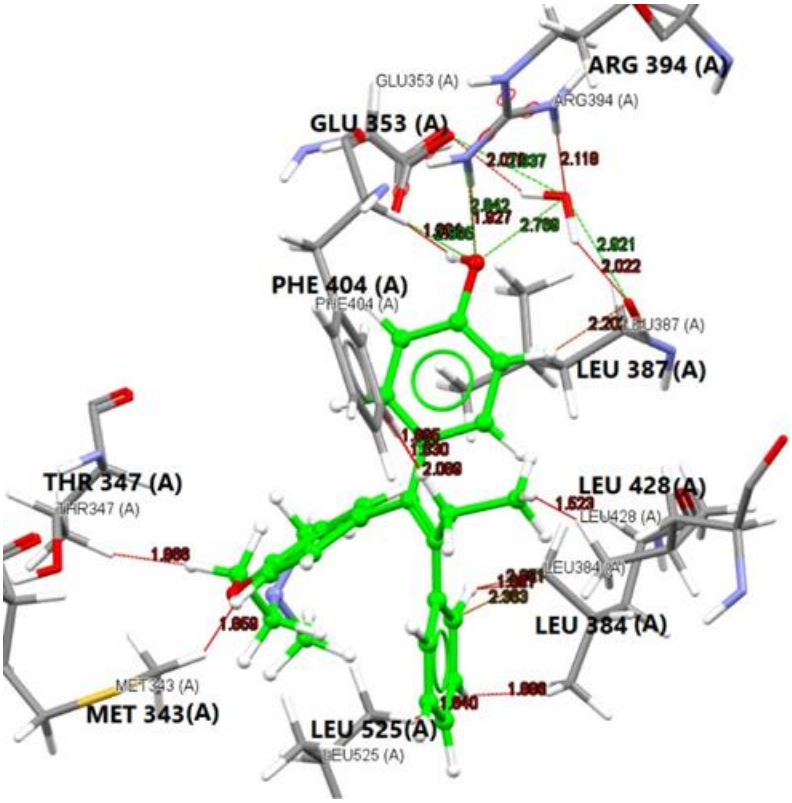

Figure 3. Interaction of 4-hydroxytamoxifen with the human estrogen receptor (PDB: 1ERR).

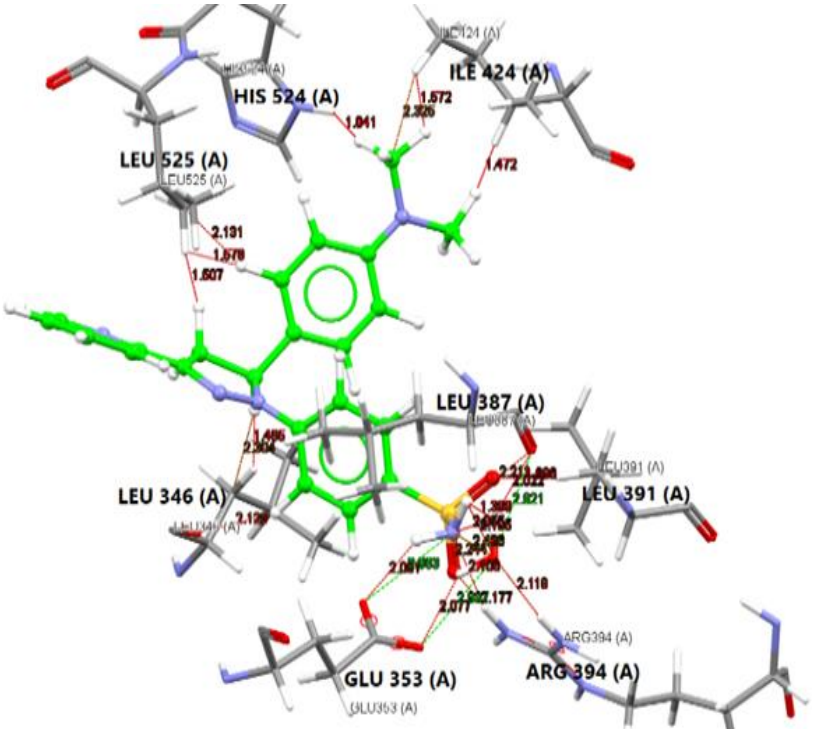

Figure 4. Interaction of compound 8 with the human estrogen receptor (PDB: 1ERR).

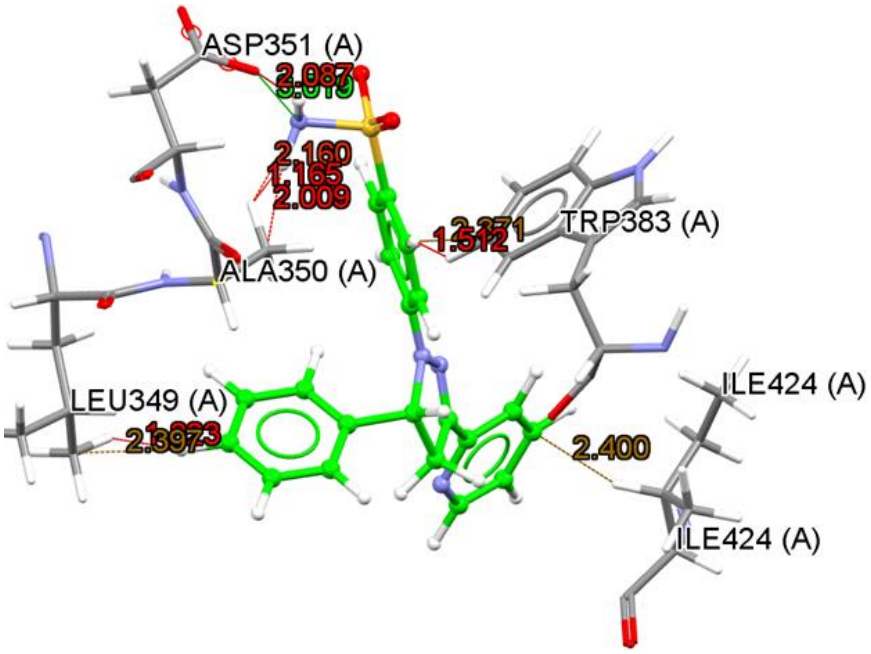

Figure 5. Interaction of compound 10 with the human estrogen receptor (PDB: 1ERR).

Analysis of anti-breast cancer activity

Cytotoxicity studies of compounds 6–10 demonstrated their potential anti-breast cancer effects. Among them, compound 9 exhibited the strongest activity, with an IC_{50} of 2.79 µM against MDA-MB-468 cells, making it approximately 5.4 times more potent than tamoxifen, which showed an IC_{50} of 15.29 µM. This indicates that compound 9 can inhibit the growth of MDA-MB-468 cancer cells at a substantially lower concentration than tamoxifen. In comparison, compounds 8 and 10 had IC_{50} values of 7.4 µM and 17.96 µM, respectively, reflecting moderate cytotoxicity. The remaining compounds displayed relatively low activity, with IC_{50} values exceeding 50 µM in both cell lines. **Table 3** summarizes the percentage of cell death for MCF-7 and MDA-MB-468 cells after 72 hours of treatment with varying concentrations of compounds 6–10, as determined by the MTT assay. Dose-response curves for tamoxifen and compound 9 in both cell lines are presented in **Figures 5–7**, while **Figures 7, 8, and 10** illustrate detailed results for compound 8.

Table 3. Comparing tamoxifen to all compounds (C6–C10) at 72 hours for cell death in MCF-7 and MDA-MB-468 cell lines.

Conc. µM	MDA-MB-468						MCF-7					
	6	7	8	9	10	Tamoxifen	6	7	8	9	10	Tamoxifen
100	59.32	55.44	60.01	95.01	55.45	97.86	40.56	49.5	91.35	58.69	92.93	96.61
50	51.32	40.42	52.36	92.36	50.76	96.92	33.32	40.32	88.08	47.98	85.16	93.31
25	42.99	30.39	45.40	85.40	44.78	92.69	20.76	30.65	77.55	40.54	69.62	88.17
12.5	31.47	27.44	30.74	80.74	30.55	68.14	17.34	22.21	67.41	30.21	49.57	62.89
6.25	26.05	18.57	27.10	77.10	20.6	55.92	10.45	14.87	49.86	20.3	35.82	62.81
3.12	19.66	13.44	11.16	71.16	10.1	48.27	5.43	10.87	23.80	14.5	27.88	41.5
1.5	8.50	2.98	4.37	64.37	3.1	41.60	3.87	3.76	17.50	6.8	27.17	40.50

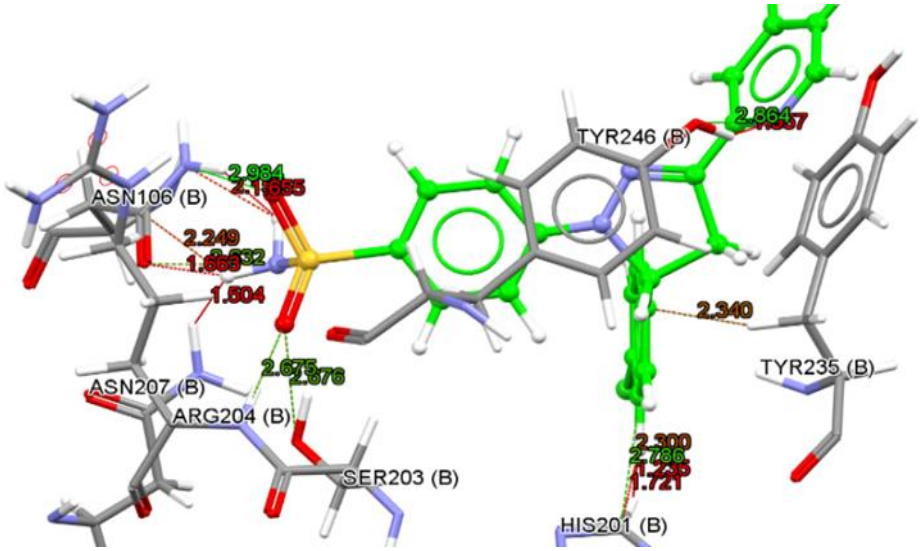

Figure 6. Interaction of compound 10 with PARP1 (PDB: 5HA9).

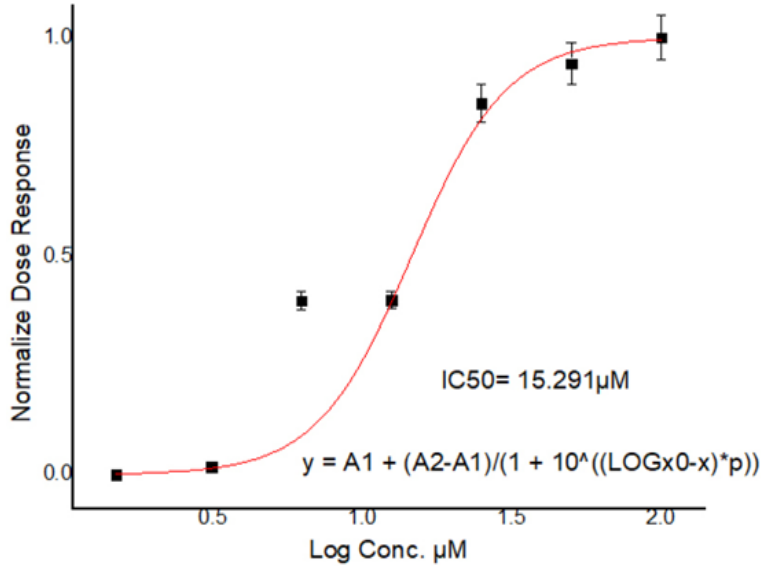

Figure 7. IC_{50} dose–response curves of tamoxifen on MDA-MB-468 cells.

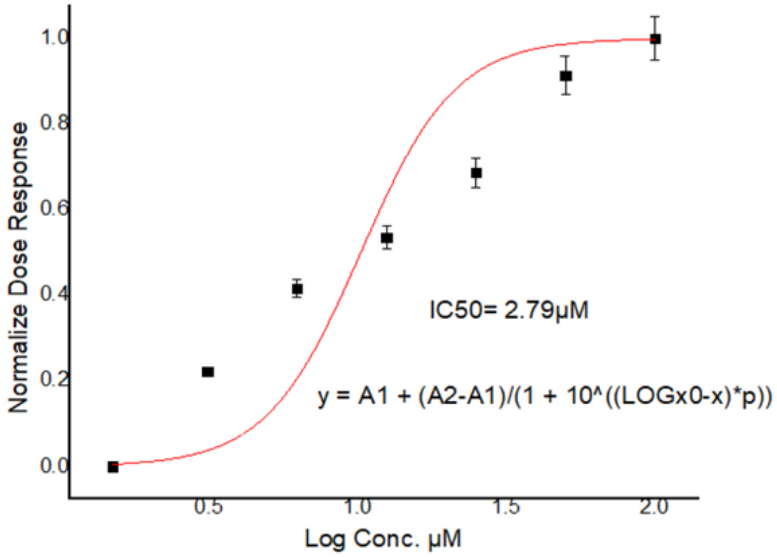

Figure 8. IC_{50} dose–response curves of compound 9 on MDA-MB-468 cells.

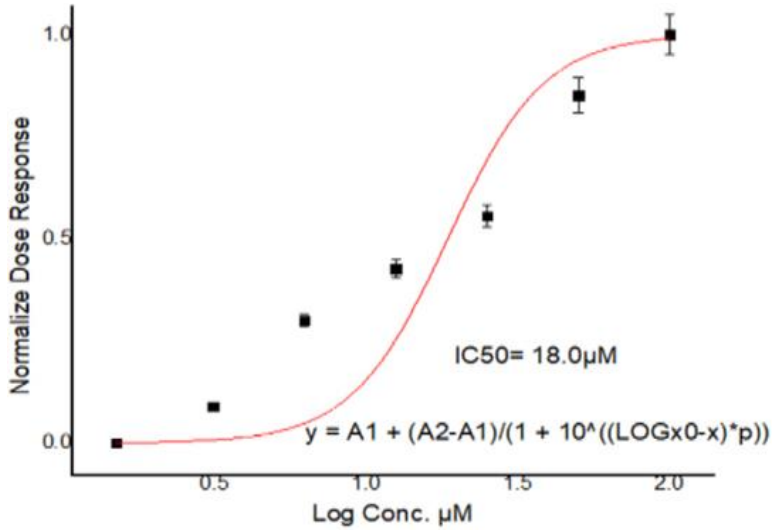

Figure 9. IC_{50} dose–response curves of tamoxifen on MCF-7 cells.

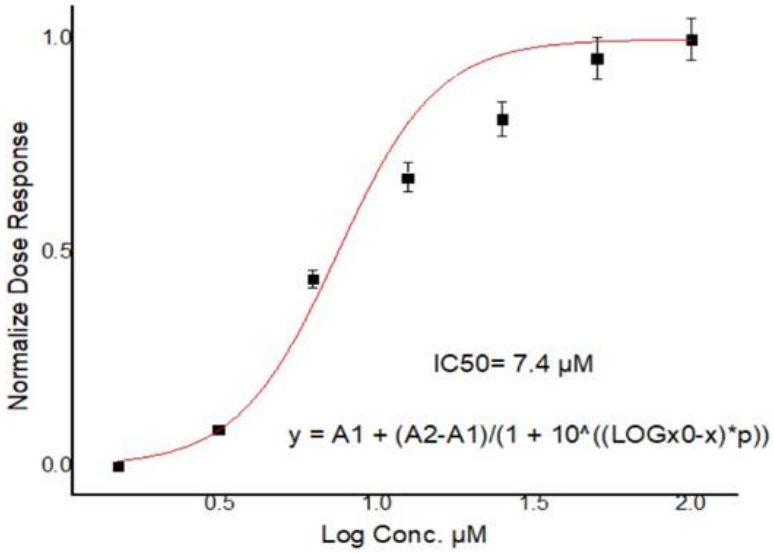

Figure 10. IC_{50} dose–response curves of compound 8 on MCF-7 cells.

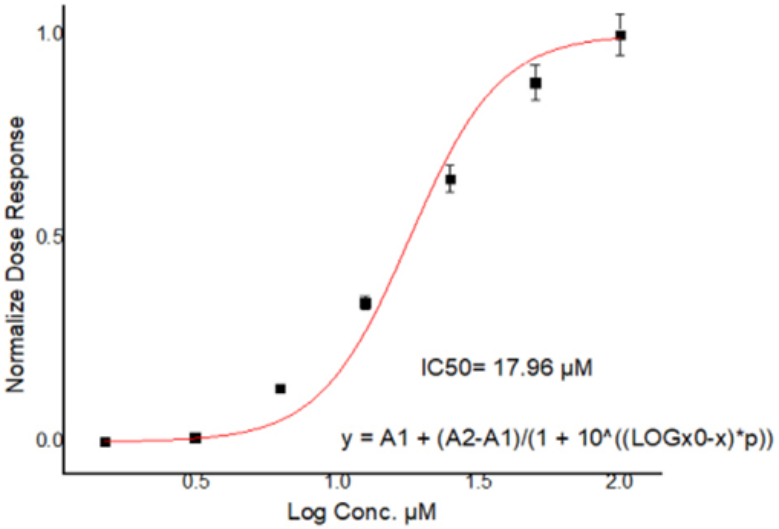

Figure 11. IC50 dose–response curves of compound 10 against the MCF-7 cell line.

Conclusion

The analysis of the synthesized compounds indicates that pyrazolines bearing sulfonamide groups exhibit remarkable anti-breast cancer activity. Docking studies revealed strong binding affinities of compounds (6–10) with both the human estrogen receptor and the PARP1 antagonist, which was further supported by in vivo results. Specifically, compound 9 showed pronounced activity against the MDA-MB-468 cell line, whereas compounds 8 and 10 were more effective against the MCF-7 cell line. Furthermore, ADME profiling confirmed that all synthesized compounds complied with Lipinski's rule of five, except for compound 7.

Acknowledgments: None

Conflict of Interest: None

Financial Support: None

Ethics Statement: None

References

1. Nepali K, Sharma S, Sharma M, Bedi PM, Dhar KL. Rational approaches, design strategies, structure-activity relationship, and mechanistic insights for anticancer hybrids. Eur J Med Chem. 2014;77:422-87. doi:10.1016/j.ejmech.2014.03.018
2. Jin C, Liang YJ, He H, Fu L. Synthesis and antitumor activity of ureas containing pyrimidinyl group. Eur J Med Chem. 2011;46(1):429-32. doi:10.1016/j.ejmech.2010.11.026
3. Din NMU, Dar RA, Rasool M, Assad A. Breast cancer detection using deep learning: Datasets, methods, and challenges ahead. Comput Biol Med. 2022;149:106073. doi:10.1016/j.compbiomed.2022.106073
4. Narzieyva DF, Jonibekov JJ. Morphological features of tumor in different treatment options for patients with locally advanced breast cancer. Middle Eur Sci Bull. 2020;7:105-7. doi:10.47494/mesb.2020.1.151
5. Tutzauer J, Sjöström M, Bendahl PO, Rydén L, Fernö M, Leeb-Lundberg LF, et al. Plasma membrane expression of G protein-coupled estrogen receptor (GPER)/G protein-coupled receptor 30 is associated with worse outcome in metachronous contralateral breast cancer. PLoS One. 2020;15(4):e0231786. doi:10.1371/journal.pone.0231786
6. Pham TH, Page YL, Percevault F, Ferriere F, Flouriot G, Pakdel F. Apigenin, a partial antagonist of the estrogen receptor, inhibits ER-positive breast cancer cell proliferation through Akt/FOXM1 signaling. Int J Mol Sci. 2021;22(1):470. doi:10.3390/ijms22010470
7. Dika E, Patrizi A, Lambertini M, Manuelpillai N, Fiorentino M, Altimari A, et al. Estrogen receptors and melanoma: A review. Cells. 2019;8(11):1463. doi:10.3390/cells8111463
8. Jacenik D, Beswick EJ, Krajewska WM, Prossnitz ER. G protein-coupled estrogen receptor in colon function, immune regulation and carcinogenesis. World J Gastroenterol. 2019;25(30):4092. doi:10.3748/wjg.v25.i30.4092
9. Maity K. Synthesis, characterization, molecular docking and evaluation of the anticancer activity of 2-pyrazoline derivatives. Asian J Pharm Pharmacol. 2019;5(5):1010-21. doi:10.31024/ajpp.2019.5.5.22
10. Zagami P, Carey LA. Triple-negative breast cancer: Pitfalls and progress. NPJ Breast Cancer. 2022;8(1):1-10. doi:10.1038/s41523-022-00468-0
11. Morais CS, Mengarda AC, Miguel FB, Enes KB, Rodrigues VC, Espírito-Santo MCC, et al. Pyrazoline derivatives as promising novel antischistosomal agents. Sci Rep. 2021;11(1):1-13. doi:10.1038/s41598-021-02792-0
12. Kiyani H, Albooyeh F, Fallahnezhad S. Synthesis of new pyrazolyl-1,3-diazabicyclo[3.1.0]hexe-3-ene derivatives. J Mol Struct. 2015;1091:163-9. doi:10.1016/j.molstruc.2015.02.069
13. Lv PC, Sun J, Luo Y, Yang Y, Zhu HL. Design, synthesis, and structure-activity relationships of pyrazole derivatives as potential FabH inhibitors. Bioorg Med Chem Lett. 2010;20(15):4657-60. doi:10.1016/j.bmcl.2010.05.105

14. Tok F, Abas BI, Çevik Ö, Koçyiğit-Kaymakçıoğlu B. Design, synthesis and biological evaluation of some new 2-pyrazoline derivatives as potential anticancer agents. Bioorg Chem. 2020;102:104063. doi:10.1016/j.bioorg.2020.104063
15. Amin KM, Eissa AA, Abou-Seri SM, Awadallah FM, Hassan GS. Synthesis and biological evaluation of novel coumarin–pyrazoline hybrids endowed with phenylsulfonyl moiety as antitumor agents. Eur J Med Chem. 2013;60:187-98. doi:10.1016/j.ejmech.2012.12.004
16. Rathore P, Yaseen S, Ovais S, Bashir R, Yaseen R, Hameed AD, et al. Synthesis and evaluation of some new pyrazoline substituted benzene sulfonylureas as potential antiproliferative agents. Bioorg Med Chem Lett. 2014;24(7):1685-91. doi:10.1016/j.bmcl.2014.02.059
17. Hamblin MR. Shining light on the head: Photobiomodulation for brain disorders. BBA Clin. 2016;6:113-24. doi:10.1016/j.bbacli.2016.09.002
18. Fadhil HR, Mahdi MF, Raauf AMR. Molecular docking, synthesis, characterization and antiproliferative evaluation of pyrazoline derivatives. Biochem Cell Arch. 2022;22(1):2927-36.
19. Raauf AM, Omar TN, Mahdi MF, Fadhil HR. Synthesis, molecular docking and anti-inflammatory evaluation of new trisubstituted pyrazoline derivatives bearing benzenesulfonamide moiety. Nat Prod Res. 2022;38(2):253-60. doi:10.1080/14786419.2022.2117174
20. Eid NM, George RF. Facile synthesis of some pyrazoline-based compounds with promising anti-inflammatory activity. Future Med Chem. 2018;10(2):183-99. doi:10.4155/fmc-2017-0144
21. Daina A, Michielin O, Zoete V. SwissADME: A free web tool to evaluate pharmacokinetics, drug-likeness and medicinal chemistry friendliness of small molecules. Sci Rep. 2017;7(1):1-13. doi:10.1038/srep42717
22. Odoemelam CS, Hunter E, Simms J, Ahmad Z, Chang MW, Percival B, Wilson PB. In silico ligand docking approaches to characterise the binding of known allosteric modulators to the glucagon-like peptide 1 receptor and prediction of ADME/Tox properties. Appl Biosci. 2022;1(2):143-62. doi:10.3390/applbiosci1020010
23. Kadela-Tomanek M, Jastrzębska M, Chrobak E, Bębenek E, Boryczka S. Chromatographic and computational screening of lipophilicity and pharmacokinetics of newly synthesized betulin–1,4-quinone hybrids. Processes. 2021;9(2):376. doi:10.3390/pr9020376